Vibroacoustic analysis of double-wall sandwich panels with viscoelastic core

Walid Larbi, Jean-François Deü, Roger Ohayon

Vibroacoustic analysis of double-wall sandwich panels with viscoelastic core

W. Larbi *, J.F. Deü, R. Ohayon

Structural Mechanics and Coupled Systems Laboratory, Conservatoire National des Arts et Métiers, 292 rue Saint-Martin, 75141 Paris Cedex 03, France

In this work, an original finite element modeling to investigate the effects of a viscoelastic layer on the sound transmission through double-wall sandwich panels is presented. This formulation is obtained from a coupled fluid–structure variational principle taking into account the frequency dependence of the viscoelastic material. The resolution approach is based on a reduced order model generated by a modal projection technique. The sound insulation of the panels is evaluated by computing its sound transmission factor using Rayleigh integral method. An efficient and inexpensive finite element for a sandwich plate with viscoelastic core is developed. Various results are presented in order to validate and illustrate the efficiency of the proposed finite element formulations.

1. Introduction

Double-wall structures are widely used in noise control due to their superiority over single-leaf structures in providing better acoustic insulation. Typical examples include double glazed windows, fuselage of airplanes, vehicles, etc. Different theoretical, experimental and numerical approaches have been investigated to predict the sound transmission through double walls with an acoustic enclosure. In [6,22,12], theoretical approaches are proposed for the derivation of the sound transmission factor of double panels of infinite size exposed to a random sound field as a function of frequency and angle of incidence. For a finite panels size, a theoretical study, based on Fourier series expansions, on the vibroacoustic performance of a rectangular double-panel partition clamp mounted in an infinite acoustic rigid baffle is presented in [35]. Experimental evaluation of sound transmission through single, double and triple glazing can be found in [28,29,33,11]. Regarding the numerical prediction approaches, several methods are available in the literature, such as the finite element method (FEM), the boundary element method (BEM), and the Statistical Energy Analysis (SEA). In [1], FEM is applied to study the viscothermal fluid effects on vibro-acoustic behavior of double elastic panels. The FEM is applied in [32] by the authors for the different layers of the sound barrier coupled to a variational BEM to account for fluid loading. In [9], the SEA is used for predicting sound transmission through double walls and for computing the non-resonant loss factor. For all these approaches, the choice of the numerical method is related to the computational cost and the frequency band to be treated.

By introducing a thin viscoelastic interlayer within the panels, a better acoustic insulation is obtained. In fact, sandwich structures with viscoelastic layer are commonly used in many systems for vibration damping and noise control. In such structures, the main energy loss mechanism is due to the transverse shear of the viscoelastic core. However, accurate modeling of structures with viscoelastic materials is difficult because the measured dynamic properties of viscoelastic material are frequency and temperature dependent. This motivated several authors to develop accurate numerical methods of modeling the effects of viscoelastic damping mechanisms which introduce frequency dependence. A review of these methods can be found in [34]. In the same context, many studies are dedicated to the development of sandwich finite element with viscoelastic core [14,7,3,31,4].

Concerning the application of these structures in noise attenuation, we can cite [15] where numerical and experimental results concerning the sound transmission through a single and a double laminated glass with Polyvinyl Butyral (PVB) viscoelastic interlayer are presented and compared. In [11], the measured sound transmission loss of multilayered structures is compared with transfer matrix method results (assuming infinite layers) and a wave based model (taking into account finite dimensions) to show the importance of the finite dimensions in a broad frequency range. The effects of viscothermal fluid in a laminated double glazing are investigated in [2] using a finite element approach.

* Corresponding author.

This work is based upon Larbi et al. [21] for vibroacoustic analysis of double-wall sandwich panels with viscoelastic core, but includes the development of an original finite element sandwich plate. In the first part of this paper, a non-symmetric finite element formulation of double-wall sandwich panels with viscoelastic core is derived from a variational principle involving structural displacement and acoustic pressure in the fluid cavity. Since the elasticity modulus of the viscoelastic core is complex and frequency dependent, this formulation is complex and nonlinear. Therefore, the direct solution of this problem can be considered only for small model sizes. This has severe limitations in attaining adequate accuracy and wider frequency ranges of interest. An original reduced order-model is then proposed to solve the problem at a lower cost. The proposed methodology, based on a normal mode expansion, requires the computation of the uncoupled structural and acoustic modes. The uncoupled structural modes are the real and undamped modes of the sandwich panels without fluid pressure loading at fluid–structure interface, whereas the uncoupled acoustic modes are the cavity modes with rigid wall boundary conditions at the fluid–structure interface. Moreover, the effects of the higher modes of each subsystem are taken into account through an appropriate so-called a priori static correction based on adding the static modes, defined as the deformation shape at every load, to the truncated bases. It is shown that the projection of the full-order coupled finite element model on the uncoupled bases, leads to a reduced order model in which the main parameters are the classical fluid–structure and residual stiffness complex coupling factors. Thanks to its reduced size, this model is proved to be very efficient for simulations of steady-state and frequency analyses of the coupled structural–acoustic system with viscoelastic damping and the computational effort is significantly reduced. As a next step, the sound transmission through double walls is investigated. When the normal velocity distribution of the panel is known, the acoustic pressure field generated in the outward direction of the two plates can be calculated with the so-called Rayleigh integral for two-dimensional sound radiation. For this purpose, it is assumed that the double wall panel is placed in an infinite baffle. The normal incidence sound transmission is chosen in order to evaluate the acoustic performances and the sound insulation of the double wall.

The second part of this work is devoted to the development of an efficient finite element sandwich plate. The model is based on the layerwise theory with a first order shear deformation in each layer. The skins are described according to the Kirchhoff–Love theory with a correction which takes into account the rotational influence of the transversal shearing in the core. A Mindlin model is used to describe the displacement field of the core. A four nodes finite element layered plate, with seven degrees-of-freedom (dof) per node, is then developed. The in-plane displacements and the rotations of the core are discretized by conforming bi-linear Lagrange shape functions, while the transverse displacement and rotations of the skins are discretized by non-conforming cubic Hermite shape functions. This choice is proved to be efficient compared to other FE models and well adapted to structural–acoustic applications.

In the last part, numerical examples are presented in order to validate and analyze results computed from the proposed formulations.

2. Finite element formulation of the coupled problem

2.1. Local equations

Consider a double-wall structure shown in Fig. 1. Each wall occupies a domain Ω_{Si}, $i \in \{1,2\}$ such that $\Omega_S = (\Omega_{S1}, \Omega_{S2})$ is a partition of the whole structure domain. A prescribed force density $\mathbf{F}^d$ is applied to the external boundary Γ_t of Ω_S and a prescribed displacement $\mathbf{u}^d$ is applied on a part Γ_u of Ω_S. The acoustic enclosure is filled with a compressible and inviscid fluid occupying the domain Ω_F. The cavity walls are rigid except those in contact with the flexible wall structures noted Σ. It should be mentioned that fluid loading on the source and receiving side of the double panel is neglected in this work. The harmonic local equations of this structural–acoustic coupled problem can be written in terms of structure displacement $\mathbf{u}$ and fluid pressure field p [19]

$$\mathrm{div}\boldsymbol{\sigma}(\mathbf{u}) + \rho_S\omega^2\mathbf{u} = \mathbf{0} \quad \text{in } \Omega_S \tag{1}$$

$$\boldsymbol{\sigma}(\mathbf{u})\mathbf{n}_S = \mathbf{F}^d \quad \text{on } \Gamma_t \tag{2}$$

$$\boldsymbol{\sigma}(\mathbf{u})\mathbf{n}_S = p\mathbf{n} \quad \text{on } \Sigma \tag{3}$$

$$\mathbf{u} = \mathbf{u}^d \quad \text{on } \Gamma_u \tag{4}$$

$$\Delta p + \frac{\omega^2}{c_F^2}p = \mathbf{0} \quad \text{in } \Omega_F \tag{5}$$

$$\nabla p \cdot \mathbf{n} = \rho_F\omega^2\mathbf{u}\cdot\mathbf{n} \quad \text{on } \Sigma \tag{6}$$

where ω is the angular frequency, $\mathbf{n}_S$ and $\mathbf{n}$ are the external unit normal to Ω_S and Ω_F; ρ_S and ρ_F are the structure and fluid mass densities; c_F is the speed of sound in the fluid; and $\boldsymbol{\sigma}$ is the structure stress tensor.

2.2. Constitutive relation for viscoelastic core

In order to provide better acoustic insulation, damped sandwich panels with a thin layer of viscoelastic core are used in this study (Fig. 1). In fact, when subjected to mechanical vibrations, the viscoelastic layer absorbs part of the vibratory energy in the form of heat. Another part of this energy is dissipated in the constrained core due to the shear motion.

The constitutive relation for a viscoelastic material subjected to a sinusoidal strain is written in the following form:

$$\boldsymbol{\sigma} = \mathbf{C}^*(\omega)\boldsymbol{\varepsilon} \tag{7}$$

where $\boldsymbol{\varepsilon}$ denote the strain tensor and $\mathbf{C}^*(\omega)$ termed the complex moduli tensor, is generally complex and frequency dependent ($*$ denotes complex quantities). It can be written as:

$$\mathbf{C}^*(\omega) = \mathbf{C}'(\omega) + i\mathbf{C}''(\omega) \tag{8}$$

where $i = \sqrt{-1}$.

Furthermore, for simplicity, a linear, homogeneous and viscoelastic core will be used in this work. In the isotropic case, the viscoelastic material is defined by a complex and frequency dependent shear modulus in the form:

$$G^*(\omega) = G'(\omega) + iG''(\omega) \tag{9}$$

where $G'(\omega)$ is know as shear storage modulus, as it is related to storing energy in the volume and $G''(\omega)$ is the shear loss modulus, which represents the energy dissipation effects. The loss factor of the viscoelastic material is defined as

$$\eta(\omega) = \frac{G''(\omega)}{G'(\omega)} \tag{10}$$

which alternatively allows writing Eq. (9) as

$$G^*(\omega) = G'(\omega)(1 + i\eta(\omega)) \tag{11}$$

The Poissons ratio v is considered real and frequency independent. The loss factor of Young's modulus E^* is the same as that of the shear modulus, which leads to:

$$E^*(\omega) = E'(\omega)(1 + i\eta(\omega)) \tag{12}$$

where $E'(\omega) = 2G'(\omega)(1+v)$.

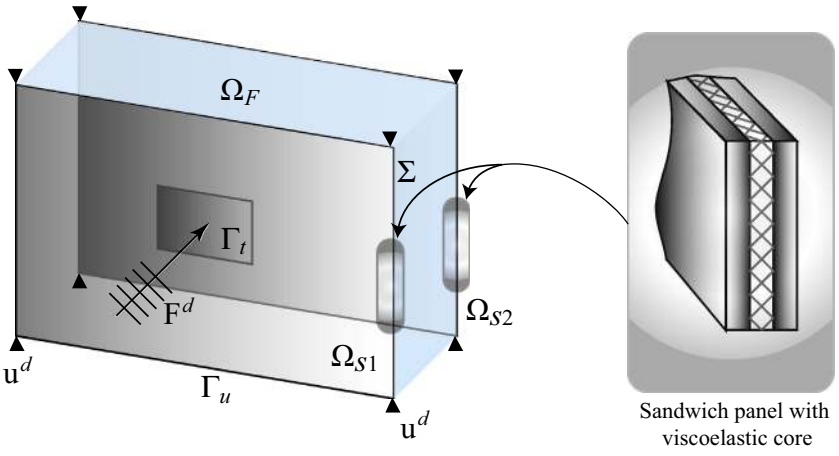

Fig. 1. Double sandwich wall structure.

With these assumptions, the stress tensor of the sandwich structure is complex and frequency dependent. It will be noted $\boldsymbol{\sigma}^*(\mathbf{u},\omega)$.

2.3. Variational formulation

The variational formulation of the problem is obtained using the test-function method. For this purpose, we introduce the spaces C_u and C_p of sufficiently smooth functions associated with the field variables $\mathbf{u}$ and p respectively.

Let $\delta\mathbf{u}$ be the test function associated to $\mathbf{u}$, belonging to the admissible space $C_u^\star = \{\delta\mathbf{u} \in C_u \,|\, \delta\mathbf{u} = \mathbf{0} \text{ on } \Gamma_u\}$. Multiplying Eq. (1) by $\delta\mathbf{u} \in C_u^\star$, applying Green's formula, and finally taking Eqs. (2) and (3) into account, we have:

$$\int_{\Omega_S} \boldsymbol{\sigma}^*(\mathbf{u},\omega) : \boldsymbol{\varepsilon}(\delta\mathbf{u})\,\mathrm{d}v - \int_\Sigma p\mathbf{n}\cdot\delta\mathbf{u}\,\mathrm{d}s - \omega^2\int_{\Omega_S}\rho_S\mathbf{u}\cdot\delta\mathbf{u}\,\mathrm{d}v = \int_{\Gamma_t}\mathbf{F}^d\cdot\delta\mathbf{u}\,\mathrm{d}s \quad \forall\delta\mathbf{u}\in C_u^\star \tag{13}$$

Similarly, let δp be the test function, associated to p, belonging to the admissible space C_p. Multiplying Eq. (5) by $\delta p \in C_p$, applying Green's formula, and finally taking Eq. (6) into account, we obtain:

$$\frac{1}{\rho_F}\int_{\Omega_F}\nabla p\cdot\nabla\delta p\,\mathrm{d}v - \omega^2\int_\Sigma \mathbf{u}\cdot\mathbf{n}\delta p\,\mathrm{d}s - \frac{\omega^2}{\rho_F c_F^2}\int_{\Omega_F} p\delta p\,\mathrm{d}v = 0 \quad \forall\delta p\in C_p \tag{14}$$

The Eqs. (13) and (14), in order to be regularized for zero frequency situation, i.e. valid for a static problem, have to be modified by adding the following constraint (see [24] for details)

$$\rho_F c_F^2\int_\Sigma \mathbf{u}\cdot\mathbf{n}\,\mathrm{d}s + \int_{\Omega_F} p\,\mathrm{d}v = 0 \tag{15}$$

When doing this, on one hand the static pressure is defined precisely by

$$p^s = -\frac{\rho_F c_F^2}{|\Omega_F|}\int_\Sigma \mathbf{u}\cdot\mathbf{n}\,\mathrm{d}s \tag{16}$$

and on the other hand, the reduced order formulation will be carried out only by projection on the physical acoustic modes [25,26].

Thus, the variational unsymmetric formulation of the fluid/elastic structure with viscoelastic damping coupled problem consists in finding $\mathbf{u}\in C_u$ such that $\mathbf{u}=\mathbf{u}^d$ on Γ_u and $p\in C_p$, satisfying Eqs. (13)–(15) with appropriate initial conditions. The symmetrization of this formulation can be obtained through the introduction of an intermediate unknown field, namely the fluid displacement potential field [24,10].

After discretizing by the finite element method the bilinear forms in Eqs. (13) and (14), we obtain the following matrix system of the coupled problem:

$$\left[\begin{pmatrix}\mathbf{K}_u^*(\omega) & -\mathbf{C}_{up}\\ \mathbf{0} & \mathbf{K}_p\end{pmatrix} - \omega^2\begin{pmatrix}\mathbf{M}_u & \mathbf{0}\\ \mathbf{C}_{up}^T & \mathbf{M}_p\end{pmatrix}\right]\begin{pmatrix}\mathbf{U}\\ \mathbf{P}\end{pmatrix} = \begin{pmatrix}\mathbf{F}\\ \mathbf{0}\end{pmatrix} \tag{17}$$

where $\mathbf{U}$ and $\mathbf{P}$ are the vectors of nodal values of $\mathbf{u}$ and p respectively. Since the complex and frequency dependent elasticity modulus of the viscoelastic core of the sandwich panels, the stiffness matrix $\mathbf{K}_u^*(\omega)$, defined by $\int_{\Omega_S}\boldsymbol{\sigma}^*(\mathbf{u},\omega):\boldsymbol{\varepsilon}(\delta\mathbf{u})\,\mathrm{d}v \Rightarrow \delta\mathbf{U}^T\mathbf{K}_u^*(\omega)\mathbf{U}$, is complex and also frequency dependent. The real and frequency-independent submatrices of Eq. (17) are given by:

$$\int_{\Omega_S}\rho_S\mathbf{u}\cdot\delta\mathbf{u}\,\mathrm{d}v \Rightarrow \delta\mathbf{U}^T\mathbf{M}_u\mathbf{U};\quad \int_{\Gamma_t}\mathbf{F}^d\cdot\delta\mathbf{u}\,\mathrm{d}s \Rightarrow \delta\mathbf{U}^T\mathbf{F}$$
$$\int_\Sigma p\mathbf{n}\cdot\delta\mathbf{u}\,\mathrm{d}s \Rightarrow \delta\mathbf{U}^T\mathbf{C}_{up}\mathbf{P};\quad \int_\Sigma \mathbf{u}\cdot\mathbf{n}\delta p\,\mathrm{d}s \Rightarrow \delta\mathbf{P}^T\mathbf{C}_{up}^T\mathbf{U}$$
$$\frac{1}{\rho_F}\int_{\Omega_F}\nabla p\cdot\nabla\delta p\,\mathrm{d}v \Rightarrow \delta\mathbf{P}^T\mathbf{K}_p\mathbf{P};\quad \frac{1}{\rho_F c_F^2}\int_{\Omega_F} p\delta p\,\mathrm{d}v \Rightarrow \delta\mathbf{P}^T\mathbf{M}_p\mathbf{P}$$

3. Reduced order model

In this section, we introduce a reduced-order formulation of the variational Eqs. (13) and (14) by a Ritz–Galerkin projection on two bases spanning the admissible spaces C_u and C_p. For C_u, we use the *in vacuo* structural modes. Concerning C_p, the basis is formed by the eigenmodes of the Helmholtz equation with rigid boundary condition. In the sequel, instead of starting from the variational formulation, we will carry the projection directly on the discretized system (17).

3.1. Eigenmodes of the structure in vacuo

In a first phase, the first N_s eigenmodes of the structure *in vacuo* are obtained from

$$\left[\mathbf{K}_u^*(\omega) - \omega^2\mathbf{M}_u\right]\mathbf{U} = \mathbf{0} \tag{18}$$

Due to the frequency dependence of the stiffness matrix, this eigenvalue problem is complex and nonlinear. It is assumed that vibrations of the damped structure can be represented in terms of the real modes of the associated undamped system if appropriate damping terms are inserted into the uncoupled modal equations

of motion [13,8]. Thus, the complex stiffness matrix is decomposed in the sum of two matrices:

$$\mathbf{K}_u^*(\omega) = \mathbf{K}_{u0} + \delta\mathbf{K}_u^*(\omega) \tag{19}$$

where $\mathbf{K}_{u0}$ is the real and frequency-independent stiffness matrix calculated with a constant Young's modulus of the viscoelastic core and $\delta\mathbf{K}_u^*(\omega)$ is the residual stiffness matrix.

The ith real eigenmode is obtained from the following equation

$$\left[\mathbf{K}_{u0} - \omega_{si}^2\mathbf{M}_u\right]\mathbf{\Phi}_{si} = \mathbf{0} \quad \text{for } i \in \{1,\ldots,N_s\} \tag{20}$$

where $(\omega_{si}, \mathbf{\Phi}_{si})$ are the natural frequency and eigenvector for the ith structural mode. These modes verify the following orthogonality properties

$$\mathbf{\Phi}_{si}^T\mathbf{M}_u\mathbf{\Phi}_{sj} = \delta_{ij} \quad \text{and} \quad \mathbf{\Phi}_{si}^T\mathbf{K}_{u0}\mathbf{\Phi}_{sj} = \omega_{si}^2\delta_{ij} \tag{21}$$

where δ_{ij} is the Kronecker symbol and $\mathbf{\Phi}_{si}$ have been normalized with respect to the structure mass matrix.

3.2. Eigenmodes of the internal acoustic cavity with rigid walls

In this second phase, the first N_f eigenmodes of the acoustic cavity with rigid boundary conditions are obtained from the following equation

$$\left[\mathbf{K}_p - \omega_{fi}^2\mathbf{M}_p\right]\mathbf{\Phi}_{fi} = \mathbf{0} \quad \text{for } i \in \{1,\ldots,N_f\} \tag{22}$$

where $(\omega_{fi}, \mathbf{\Phi}_{fi})$ are the natural frequency and eigenvector for the ith acoustic mode. These modes verify the following orthogonality properties

$$\mathbf{\Phi}_{fi}^T\mathbf{M}_p\mathbf{\Phi}_{fj} = \delta_{ij} \quad \text{and} \quad \mathbf{\Phi}_{fi}^T\mathbf{K}_p\mathbf{\Phi}_{fj} = \omega_{fi}^2\delta_{ij} \tag{23}$$

where $\mathbf{\Phi}_{fi}$ have been normalized with respect to the fluid mass matrix.

3.3. Modal expansion of the general problem

By introducing the matrices $\mathbf{\Phi}_s = [\mathbf{\Phi}_{s1} \cdots \mathbf{\Phi}_{sN_s}]$ of size $(M_s \times N_s)$ and $\mathbf{\Phi}_f = \left[\mathbf{\Phi}_{f1} \cdots \mathbf{\Phi}_{fN_f}\right]$ of size $(M_f \times N_f)$ corresponding to the uncoupled bases (M_s and M_f are the total number of degrees of freedom in the finite elements model associated to the structure and the acoustic domains respectively), the displacement and pressure are sought as

$$\mathbf{U} = \mathbf{\Phi}_s\mathbf{q}_s(t) \quad \text{and} \quad \mathbf{P} = \mathbf{\Phi}_f\mathbf{q}_f(t) \tag{24}$$

where the vectors $\mathbf{q}_s = \left[q_{s1} \cdots q_{sN_s}\right]^T$ and $\mathbf{q}_f = \left[q_{f1} \cdots q_{fN_f}\right]^T$ are the modal amplitudes of the structure displacement and the fluid pressure respectively.

Substituting these relations into Eq. (17) and pre-multiplying the first row by $\mathbf{\Phi}_s^T$ and the second one by $\mathbf{\Phi}_f^T$, we obtain the equation

$$\begin{bmatrix} \mathbf{\Phi}_s^T\left(\mathbf{K}_{u0} + \delta\mathbf{K}_u^*(\omega)\right)\mathbf{\Phi}_s & -\mathbf{\Phi}_s^T\mathbf{C}_{up}\mathbf{\Phi}_f \\ \mathbf{0} & \mathbf{\Phi}_f^T\mathbf{K}_p\mathbf{\Phi}_f \end{bmatrix}\begin{bmatrix}\mathbf{q}_s\\ \mathbf{q}_f\end{bmatrix} - \omega^2\begin{bmatrix} \mathbf{\Phi}_s^T\mathbf{M}_u\mathbf{\Phi}_s & \mathbf{0} \\ \mathbf{\Phi}_f^T\mathbf{C}_{up}^T\mathbf{\Phi}_s & \mathbf{\Phi}_f^T\mathbf{M}_p\mathbf{\Phi}_f \end{bmatrix}\begin{bmatrix}\mathbf{q}_s\\ \mathbf{q}_f\end{bmatrix} = \begin{bmatrix}\mathbf{\Phi}_s^T\mathbf{F}\\ \mathbf{0}\end{bmatrix} \tag{25}$$

This matrix equation represents the reduced order model of the structural acoustic problem with viscoelastic damping treatments. If only few modes are kept for the projection, the size of this reduced order model $(N_s \times N_f)$ is much more smaller than the initial one $(M_s \times M_f)$. Eq. (25) can be also written in the following form of coupled differential equations:

- N_s mechanical equations

$$-\omega^2 q_{si} + \sum_{k=1}^{N_s}\gamma_{ik}^*(\omega)q_{si} + \omega_{si}^2 q_{si} - \sum_{j=1}^{N_f}\beta_{ij}q_{fj} = F_i \tag{26}$$

- N_f acoustic equations

$$-\omega^2 q_{fi} + \omega_{fi}^2 q_{fi} - \omega^2\sum_{j=1}^{N_s}\beta_{ij}q_{sj} = 0 \tag{27}$$

where $F_i(t) = \mathbf{\Phi}_{si}^T\mathbf{F}$ is the mechanical excitation of the i*th* mode; $\beta_{ij} = \mathbf{\Phi}_{si}^T\mathbf{C}_{up}\mathbf{\Phi}_{fj}$ is the fluid structure coupling coefficient and $\gamma_{ik}^*(\omega) = \mathbf{\Phi}_{si}^T\delta\mathbf{K}_u^*(\omega)\mathbf{\Phi}_{sk}$ the reduced residual stiffness complex coefficient.

At each frequency step, the reduced system (Eqs. (26) and (27)) is solved by updating $\gamma_{ik}^*(\omega)$. After determining the complex amplitude vectors q_{si} and q_{fi}, the displacement and pressure fields are reconstructed using the modal expansion (Eq. (24)).

3.4. Modal truncation augmentation method with static corrections

The process of mode truncation introduces some errors in the response that can be controlled or minimized by a modal truncation augmentation method. In this method, the effects of the truncated modes are considered by their static effect only.

First the applied loading vector $\mathbf{F}$ is composed as:

$$\mathbf{F} = \sum_{i=1}^{L}\alpha_i(t)\mathbf{F}_{0i} \tag{28}$$

where $\mathbf{F}_{0i}$ is the invariant spatial portion and $\alpha_j(t)$ is the time varying portion. For each invariant spatial load, the static modal eigenvector $\mathbf{\Psi}_{si}$ is given by:

$$\mathbf{\Psi}_{si} = \mathbf{K}_{u0}^{-1}\mathbf{F}_{0i} \tag{29}$$

The truncated basis containing the real and undamped structure modes is enriched by the static modal eigenvectors such that

$$\bar{\mathbf{\Phi}}_s = [\mathbf{\Phi}_{s1} \cdots \mathbf{\Phi}_{sN_s}, \mathbf{\Psi}_{si}, \cdots \mathbf{\Psi}_{sl}] = [\mathbf{\Phi}_s\,\mathbf{\Psi}_s] \tag{30}$$

The truncated fluid basis is enriched with the static pressure $\mathbf{P}_s$ computed from Eq. (16):

$$\bar{\mathbf{\Phi}}_f = \left[\mathbf{\Phi}_f\,\mathbf{P}_s\right] \tag{31}$$

Thus, the displacement and pressure are sought as

$$\mathbf{U} = \mathbf{\Phi}_s\mathbf{q}_s(t) + \mathbf{\Psi}_s\mathbf{q}_s^0(t) \quad \text{and} \quad \mathbf{P} = \mathbf{\Phi}_f\mathbf{q}_f(t) + \mathbf{P}_s q_f^0(t) \tag{32}$$

where the vectors $\mathbf{q}_s^0$ and q_f^0 are the quasi-static modal amplitudes of the structure displacement and the fluid pressure respectively.

Substituting these relations (Eq. (32)) into Eq. (17) and pre-multiplying the first row by $[\mathbf{\Phi}_s\,\mathbf{\Psi}_s]^T$ and the second one by $\left[\mathbf{\Phi}_f\,\mathbf{P}_s\right]^T$, we obtain coupled differential equations enriched with fluid and structure static modes similar than Eqs. (26) and (27) which are not shown here for the sake of brevity.

4. Acoustic indicators

In order to evaluate the acoustic performances and the sound insulation property of the double-wall sandwich panels, the radiated sound power (Π_t) and the normal incidence sound transmission loss (nSTL) are used as acoustic indicators in this work.

4.1. Radiated sound power

The radiated (or transmitted) sound power through the area S_2 of the panel Ω_{S2} is given by:

$$\Pi_t = \frac{1}{2}\mathrm{Re}\left(\int_{S_2} p(G)\, v_n^{\star}(G)\mathrm{d}S\right) \tag{33}$$

where G is a point on the plate surface Ω_{S2}, p is the sound pressure applied as an external loading, v_n is the normal velocity ($\star$ denotes the complex conjugate) and Re is the real part of the expression.

For a flat plate embedded in an infinite rigid plane baffle and radiating in a semi infinite fluid, p can be obtained using the Rayleigh Integral [12]:

$$p(\omega, M) = \rho_0 \frac{i\omega}{2\pi}\int_{S_2} v_n(\omega, G)\frac{e^{-ikr}}{r}\mathrm{d}S \tag{34}$$

where ρ_0 is the mass density of the external acoustic domain, k is the wave number expressed as ω/c_0, c_0 is the acoustic speed of sound, M is a point inside the external acoustic domain and $v_n(\omega, G)$ is the normal velocity at point G expressed as $v_n(\omega, G) = \mathbf{v}(G, \omega)\cdot\mathbf{n}_S$. Note that the normal velocity distribution on the structure can be easily obtained from the previous finite element formulation.

The baffled panel is divided into a grid of R rectangular elements with equal size whose transverse vibrations are specified in terms of the normal velocities at their center positions. Assuming that the dimensions of the element are small compared with both the structural wavelength and the acoustic wavelength, the total radiated sound power (Eq. (33)) can then be expressed as the summation of the powers radiated by each element, so that

$$\Pi_t = \frac{S_e}{2}\mathrm{Re}\left(\mathbf{v}_n^H\mathbf{p}\right) \tag{35}$$

where the superscript H denotes the hermitian transpose, $\mathbf{v}_n$ and $\mathbf{p}$ are the vectors of complex amplitudes of the normal volume velocity and acoustic pressure in all elements and S_e is the area of each element. The pressure on each element is generated by the vibrations of all elements of the panel. The vector of sound pressure can therefore be expressed by the impedance matrix relation

$$\mathbf{p} = \mathbf{Z}\mathbf{v}_n \tag{36}$$

where $\mathbf{Z}$ is the matrix incorporating the point and transfer acoustic impedance terms over the grid of elements into which the panel has been subdivided: $Z_{ij} = (i\omega\rho_0 S_e/2\pi r_{ij})e^{-ikr_{ij}}$ (r_{ij} is the distance between the centers of the i-th and j-th elements). Note that, because of reciprocity, the impedance matrix $\mathbf{Z}$ is symmetric. Substituting Eq. (36) into the expression for the total radiated sound power given in Eq. (35), we obtain

$$\Pi_t = \frac{S_e}{2}\mathrm{Re}\left(\mathbf{v}_n^H\mathbf{Z}\mathbf{v}_n\right) = \frac{S_e}{4}\mathrm{Re}\left(\mathbf{v}_n^H\left[\mathbf{Z}+\mathbf{Z}^H\right]\mathbf{v}_n\right) = \mathbf{v}_n^H\mathbf{R}\mathbf{v}_n \tag{37}$$

The matrix $\mathbf{R}$ is defined as the "radiation resistance matrix" for the elementary radiators which, for the baffled panel, is given by

$$\mathbf{R} = \frac{\omega^2\rho_0 S_e^2}{4\pi c_0}\begin{bmatrix} 1 & \frac{\sin(kr_{12})}{kr_{12}} & \cdots & \frac{\sin(kr_{1R})}{kr_{1R}} \\ \frac{\sin(kr_{21})}{kr_{21}} & 1 & \cdots & \frac{\sin(kr_{2R})}{kr_{2R}} \\ \vdots & \vdots & \ddots & \vdots \\ \frac{\sin(kr_{R1})}{kr_{R1}} & \frac{\sin(kr_{R2})}{kr_{R2}} & \cdots & 1 \end{bmatrix} \tag{38}$$

This method can be applied to any plane surface in an infinite baffle, independently of the boundary conditions. It only requires the knowledge of the surface geometry, the characteristics of the fluid and the velocity field distribution. In this work, a finite element approach is used to evaluate this velocity field by using a sufficient number of discrete radiating elements according to the smallest wavelength to be observed.

4.2. Normal incidence sound transmission loss

The normal incidence sound transmission of the double-wall sandwich panels is investigated in this section using Rayleigh Integral method described above. It is evaluated using the following formula:

$$nSTL = 10Log\frac{\Pi_i}{\Pi_t} \tag{39}$$

where Π_i and Π_t are the incident and transmitted acoustic power respectively. For normal plane wave applied to plate Ω_{S1}, the incident sound power is given by:

$$\Pi_i = \frac{|P_{inc}|^2 S_1}{2\rho_0 c_0} \tag{40}$$

where P_{inc} represents the normal incident sound pressure amplitude and S_1 is the area of the whole panel Ω_{S1}.

5. Finite element development of sandwich plate with viscoelastic core

This section is devoted to the development of an efficient finite element for a sandwich plate with viscoelastic core. The considered three layers plate is shown in Fig. 2. The faces layers (1) and (3) are homogeneous, orthotropic and linearly elastic, with thickness h_1 and h_3. The core (2) is linearly viscoelastic with thickness, noted h_2, non negligible relative to that of the face layers.

5.1. Kinematic assumptions

The layerwise theory proposed in this paper is based on the assumption of a first order shear deformation theory in the core and the usual Kirchhoff–Love assumptions are made for the face layers. The other assumptions used in this study are the following:

- the cross section of each layer remains plane after deformation and the stress in the normal direction is negligeable ($\sigma_{zz} = 0$);
- the core contributes by transversal shear stresses;
- the transversal shear stresses are neglected in the faces; and

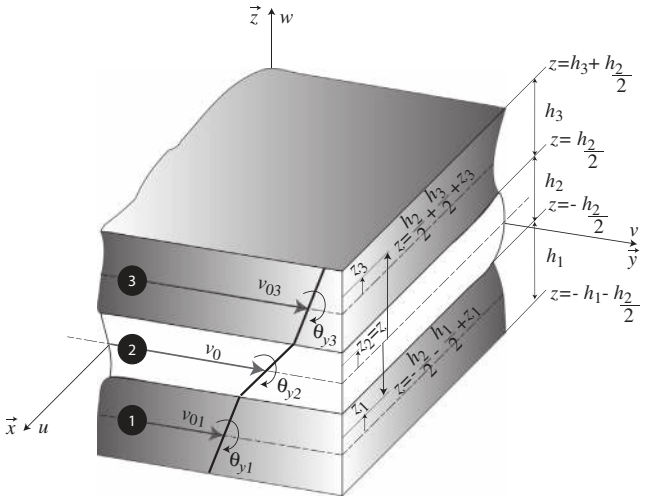

Fig. 2. Kinematic of the three layers sandwich plate.

- the transverse displacement, w, of all points on any cross-section of the sandwich plate is considered to be equal.

Following the above assumptions, the displacement field of the faces is built using the Love-Kirchhoff's assumptions but is corrected to account for the rotational influence of the transversal shearing in the core. The Mindlin assumption is used to describe the kinematic of the core.

Thus, the local displacement fields $(u_i,\ v_i,\ w_i)$ in the directions of the x, y and z axes within the ith layer can be described by the displacements $u_{0i},\ v_{0i}$ and w of the local layer middle surface $(z_i = 0)$ and a rotations θ_{xi} and θ_{yi} about the y and x axes, respectively:

$$u_i = u_{0i}(x,y) + z_i\theta_{xi}(x,y) \tag{41a}$$
$$v_i = v_{0i}(x,y) + z_i\theta_{yi}(x,y) \tag{41b}$$
$$w_i = w(x,y) \tag{41c}$$

where z_i is the local ith layer z coordinate as $-\frac{h_i}{2} \leqslant z_i \leqslant \frac{h_i}{2}$.

The continuity of the inplane displacements $(u,\ v)$ at the interfaces of the layers leads to the following relationships:

$$u_{01} = u_{02} - \frac{h_2}{2}\theta_{x2} - \frac{h_1}{2}\theta_{x1}; \quad v_{01} = v_{02} - \frac{h_2}{2}\theta_{y2} - \frac{h_1}{2}\theta_{y1} \tag{42a}$$
$$u_{03} = u_{02} + \frac{h_2}{2}\theta_{x2} + \frac{h_3}{2}\theta_{x3}; \quad v_{03} = v_{02} + \frac{h_2}{2}\theta_{y2} + \frac{h_3}{2}\theta_{y3} \tag{42b}$$

By introducing the global coordinate z showing in Fig. 2, neglecting the transversal shear stresses in the faces which allows $\theta_{x1} = \theta_{x3} = -\frac{\partial w}{\partial x}$ and $\theta_{y1} = \theta_{y3} = -\frac{\partial w}{\partial y}$, and using the above continuity relations, the local displacement fields can be written as:

$$\begin{cases} u_i = u_0 - z\frac{\partial w}{\partial x} + t_i\varphi_x \\ v_i = v_0 - z\frac{\partial w}{\partial y} + t_i\varphi_y \\ w_i = w(x,y) \end{cases} \text{ for } i = 1,3 \quad \text{and} \quad \begin{cases} u_2 = u_0 - z\frac{\partial w}{\partial x} + z\varphi_x \\ v_2 = v_0 - z\frac{\partial w}{\partial y} + z\varphi_y \\ w_2 = w(x,y) \end{cases} \tag{43}$$

where $u_0 = u_{02},\ v_0 = v_{02},\ t_1 = -\frac{h_2}{2}$ and $t_3 = \frac{h_2}{2}$ and the following rotations are introduced: $\varphi_x = \frac{\partial w}{\partial x} + \theta_{x2}$ and $\varphi_y = \frac{\partial w}{\partial y} + \theta_{y2}$.

5.2. Strain–displacements relations

For each layer i, the state of the in-plane strain $\boldsymbol{\varepsilon}^{(i)} = \left[\varepsilon_{xx}^{(i)} \quad \varepsilon_{yy}^{(i)} \quad 2\varepsilon_{xy}^{(i)}\right]^T$ is equal to the sum of the middle surface strain $\boldsymbol{\epsilon} = [\epsilon_{xx} \quad \epsilon_{yy} \quad \epsilon_{xy}]^T$ (membrane), the strain due to the change of curvature $\boldsymbol{\kappa} = [\kappa_{xx} \quad \kappa_{yy} \quad \kappa_{xy}]^T$ and the strain due to the rotational effect $\boldsymbol{\varphi} = [\varphi_{xx} \quad \varphi_{yy} \quad \varphi_{xy}]^T$:

$$\boldsymbol{\varepsilon}^{(i)} = \boldsymbol{\epsilon} - z\boldsymbol{\kappa} + t_i\boldsymbol{\varphi} \quad \text{for } i = 1,3 \quad \text{and} \quad \boldsymbol{\varepsilon}^{(2)} = \boldsymbol{\epsilon} - z\boldsymbol{\kappa} + z\boldsymbol{\varphi} \tag{44}$$

where the middle surface strain, curvatures and rotations are defined by:

$$\begin{aligned} \epsilon_{xx} &= \frac{\partial u_0}{\partial x}, \quad \kappa_{xx} = \frac{\partial^2 w}{\partial x^2}, \quad \varphi_{xx} = \frac{\partial \varphi_x}{\partial x} \\ \epsilon_{yy} &= \frac{\partial v_0}{\partial y}, \quad \kappa_{yy} = \frac{\partial^2 w}{\partial y^2}, \quad \varphi_{yy} = \frac{\partial \varphi_y}{\partial y} \\ \epsilon_{xy} &= \frac{\partial u_0}{\partial y} + \frac{\partial v_0}{\partial x}, \quad \kappa_{xy} = 2\frac{\partial^2 w}{\partial x \partial y}, \quad \varphi_{xy} = \frac{\partial \varphi_x}{\partial y} + \frac{\partial \varphi_y}{\partial x} \end{aligned} \tag{45}$$

For the core (2), additional strain related to the shear effect $\boldsymbol{\gamma}^{(2)} = \left[\gamma_{xz}^{(2)} \quad \gamma_{yz}^{(2)}\right]^T$ is added with $\gamma_{xz}^{(2)} = \varphi_x$ and $\gamma_{yz}^{(2)} = \varphi_y$.

The strain components can be rewritten in the following matrix form

$$\boldsymbol{\varepsilon} = \mathbf{D}_\varepsilon \begin{bmatrix} u_0 \\ v_0 \\ w \\ \frac{\partial w}{\partial x} \\ \frac{\partial w}{\partial y} \\ \varphi_x \\ \varphi_y \end{bmatrix} \quad \text{and} \quad \boldsymbol{\gamma}^{(2)} = \mathbf{D}_\gamma \begin{bmatrix} u_0 \\ v_0 \\ w \\ \frac{\partial w}{\partial x} \\ \frac{\partial w}{\partial y} \\ \varphi_x \\ \varphi_y \end{bmatrix} \tag{46}$$

with $\boldsymbol{\varepsilon} = \left[\epsilon_{xx} \quad \epsilon_{yy} \quad \epsilon_{xy} \quad \kappa_{xx} \quad \kappa_{yy} \quad \kappa_{xy} \quad \varphi_{xx} \quad \varphi_{yy} \quad \varphi_{xy}\right]^T$ and the gradient operators $\mathbf{D}_\varepsilon$ and $\mathbf{D}_\gamma$ are defined by

$$\mathbf{D}_\varepsilon = \begin{bmatrix} \frac{\partial}{\partial x} & 0 & 0 & 0 & 0 & 0 & 0 \\ 0 & \frac{\partial}{\partial x} & 0 & 0 & 0 & 0 & 0 \\ \frac{\partial}{\partial y} & \frac{\partial}{\partial x} & 0 & 0 & 0 & 0 & 0 \\ 0 & 0 & 0 & \frac{\partial}{\partial x} & 0 & 0 & 0 \\ 0 & 0 & 0 & 0 & \frac{\partial}{\partial y} & 0 & 0 \\ 0 & 0 & 0 & \frac{\partial}{\partial y} & \frac{\partial}{\partial x} & 0 & 0 \\ 0 & 0 & 0 & 0 & 0 & \frac{\partial}{\partial x} & 0 \\ 0 & 0 & 0 & 0 & 0 & 0 & \frac{\partial}{\partial y} \\ 0 & 0 & 0 & 0 & 0 & \frac{\partial}{\partial y} & \frac{\partial}{\partial x} \end{bmatrix} \quad \text{and} \quad \mathbf{D}_\gamma = \begin{bmatrix} 0 & 0 & 0 & 0 & 0 & 1 & 0 \\ 0 & 0 & 0 & 0 & 0 & 0 & 1 \end{bmatrix}$$

5.3. Degrees-of-freedom and shape functions

Consider a rectangular element of a plate coinciding with the xy plane as shown in Fig. 3. Each node n $(n = 1,2,3,4)$, have seven degrees-of-freedom to describe the middle surface displacements u_{0n}, v_{0n} and w_n along the x, y and z directions, the rotation of the faces about the y axis, $\frac{\partial w_n}{\partial x}$, and the rotation about the x axis, $\frac{\partial w_n}{\partial y}$, and the shearing rotations of the core about the y axis, φ_{xn}, and about the x axis, φ_{yn}.

The nodal displacement vector are defined below as $\mathbf{U}_n$. The element displacement will, as usual, be given by a listing of the nodal displacements, now totaling twenty-eight

$$\mathbf{U}^e = \begin{bmatrix} \mathbf{U}_1 \\ \mathbf{U}_2 \\ \mathbf{U}_3 \\ \mathbf{U}_4 \end{bmatrix}, \quad \mathbf{U}_n = \begin{bmatrix} u_{0n} \\ v_{0n} \\ w_n \\ \frac{\partial w_n}{\partial x} \\ \frac{\partial w_n}{\partial y} \\ \varphi_{xn} \\ \varphi_{yn} \end{bmatrix}, \quad n = 1,2,3,4 \tag{47}$$

The present element is non-conforming (i.e. it does not satisfy normal slope compatibility) but it exhibits good convergence for the linear case [36]. The displacements u_0 and v_0 and the rotations of the core φ_x and φ_y are assumed to vary linearly along the axial co-ordinate x and y and they are discretized by Lagrange bi-linear

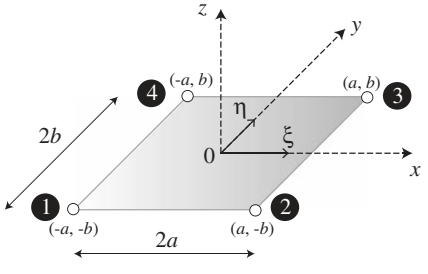

Fig. 3. Geometrical data of the quadrilateral plate element.

shape functions, while the transverse displacement w and the rotations $\frac{\partial w}{\partial x}$ and $\frac{\partial w}{\partial y}$ are described by nonconforming Hermite cubic polynomial derived by Melosh [23]. Thus, the elementary middle surface displacements and rotations of the plate are given in terms of the nodal degrees-of-freedom by

$$\begin{bmatrix} u_0^e \\ v_0^e \\ w^e \\ \frac{\partial w^e}{\partial x} \\ \frac{\partial w^e}{\partial y} \\ \varphi_x^e \\ \varphi_y^e \end{bmatrix} = \mathbf{N}(x,y)\mathbf{U}^e \tag{48}$$

where the interpolation matrix is defined by

$$\mathbf{N} = [\,\mathbf{N}_1 \quad \mathbf{N}_2 \quad \mathbf{N}_3 \quad \mathbf{N}_4\,] \tag{49}$$

and

$$\mathbf{N}_n = \begin{bmatrix} N_n^\ell & 0 & 0 & 0 & 0 & 0 & 0 \\ 0 & N_n^\ell & 0 & 0 & 0 & 0 & 0 \\ 0 & 0 & N_n^{c1} & N_n^{c2} & N_n^{c3} & 0 & 0 \\ 0 & 0 & \frac{\partial N_n^{c1}}{\partial x} & \frac{\partial N_n^{c2}}{\partial x} & \frac{\partial N_n^{c3}}{\partial x} & 0 & 0 \\ 0 & 0 & \frac{\partial N_n^{c1}}{\partial y} & \frac{\partial N_n^{c2}}{\partial y} & \frac{\partial N_n^{c3}}{\partial y} & 0 & 0 \\ 0 & 0 & 0 & 0 & 0 & N_n^\ell & 0 \\ 0 & 0 & 0 & 0 & 0 & 0 & N_n^\ell \end{bmatrix}, \quad n = 1,2,3,4 \tag{50}$$

with the following linear N_n^ℓ and cubic N_n^{c1}, N_n^{c2} and N_n^{c3} $(n = 1,2,3,4)$ shape functions given in the reference element [36]

$$N_n^\ell = \frac{1}{4}\xi_n\eta_n(\xi+\xi_n)(\eta+\eta_n) \tag{51a}$$

$$N_n^{c1} = \frac{1}{8}(1+\xi\xi_n)(1+\eta\eta_n)(2+\xi\xi_n+\eta\eta_n-\xi^2-\eta^2) \tag{51b}$$

$$N_n^{c2} = \frac{1}{8}\xi_n(\xi\xi_n-1)(1+\eta\eta_n)(1+\xi\xi_n)^2 \tag{51c}$$

$$N_n^{c3} = \frac{1}{8}\eta_n(\eta\eta_n-1)(1+\xi\xi_n)(1+\eta\eta_n)^2 \tag{51d}$$

in which $\xi = \frac{x}{a}$ and $\eta = \frac{y}{b}$ are the elementary co-ordinates that varie from -1 (when $x = -a$ for ξ and $y = -b$ for η) to 1 (when $x = a$ for ξ and $y = b$ for η), $\xi_n = \frac{x_n}{a}$ and $\eta_n = \frac{y_n}{b}$, where x_n and y_n correspond to the node n co-ordinates along the directions x and y, respectively, as shown in Fig. 3.

Moreover, elementary strain vectors $\boldsymbol{\varepsilon}^e$ and $\boldsymbol{\gamma}^e$ can be expressed by

$$\boldsymbol{\varepsilon}^e = \mathbf{B}_\varepsilon\mathbf{U}^e \quad \text{and} \quad \boldsymbol{\gamma}^e = \mathbf{B}_\gamma\mathbf{U}^e \tag{52}$$

with the following discretized gradient operator

$$\mathbf{B}_\varepsilon = \mathbf{D}_\varepsilon\mathbf{N} \quad \text{and} \quad \mathbf{B}_\gamma = \mathbf{D}_\gamma\mathbf{N} \tag{53}$$

5.3.1. Elementary mass and stiffness matrices

The interpolations of displacements and strains presented in the previous section are used to express the elementary mass and stiffness matrices of the composite laminate plate.

The mass matrix is evaluated without neglecting rotational inertia. Using its definition given in the variational formulation $(\int_{\Omega_S}\rho_S\mathbf{u}\cdot\delta\mathbf{u}\,\mathrm{d}v)$, and combining Eqs. (43) and (48), the elementary mass matrix is defined by

$$\mathbf{M}_u^e = \sum_{i=1}^{3}\mathbf{M}_{ui}^e$$

where

$$\mathbf{M}_{ui}^e = \int_{-1}^{1}\int_{-1}^{1}\mathbf{N}^T\mathbf{I}_i\mathbf{N}J(\xi,\eta)\,\mathrm{d}\xi\mathrm{d}\eta \tag{54}$$

and where J is the Jacobien determinant of the transformation and $\mathbf{I}_i$ is the composite inertia matrix given by

$$\mathbf{I}_i = \begin{bmatrix} I_0^{(i)} & 0 & 0 & -I_1^{(i)} & 0 & t_iI_0^{(i)} & 0 \\ 0 & I_0^{(i)} & 0 & 0 & -I_1^{(i)} & 0 & t_iI_0^{(i)} \\ 0 & 0 & I_0^{(i)} & 0 & 0 & 0 & 0 \\ -I_1^{(i)} & 0 & 0 & I_2^{(i)} & 0 & -t_iI_1^{(i)} & 0 \\ 0 & -I_1^{(i)} & 0 & 0 & I_2^{(i)} & 0 & -t_iI_1^{(i)} \\ t_iI_0^{(i)} & 0 & 0 & -t_iI_1^{(i)} & 0 & t_i^2I_0^{(i)} & 0 \\ 0 & t_iI_0^{(i)} & 0 & 0 & -t_iI_1^{(i)} & 0 & t_i^2I_0^{(i)} \end{bmatrix} \quad \text{for } i = 1,3 \tag{55}$$

and

$$\mathbf{I}_2 = \begin{bmatrix} I_0^{(2)} & 0 & 0 & -I_1^{(2)} & 0 & I_1^{(2)} & 0 \\ 0 & I_0^{(2)} & 0 & 0 & -I_1^{(2)} & 0 & I_1^{(2)} \\ 0 & 0 & I_0^{(2)} & 0 & 0 & 0 & 0 \\ -I_1^{(2)} & 0 & 0 & I_2^{(2)} & 0 & -I_2^{(2)} & 0 \\ 0 & -I_1^{(2)} & 0 & 0 & I_2^{(2)} & 0 & -I_2^{(2)} \\ I_1^{(2)} & 0 & 0 & -I_2^{(2)} & 0 & I_2^{(2)} & 0 \\ 0 & I_1^{(2)} & 0 & 0 & -I_2^{(2)} & 0 & I_2^{(2)} \end{bmatrix} \tag{56}$$

in which the zero $I_0^{(i)}$, first $I_1^{(i)}$ and second $I_2^{(i)}$ mass moments of inertia are given by

$$I_0^{(i)} = \rho_S^{(i)}(z_i - z_{i-1}), \quad I_1^{(i)} = \frac{\rho_S^{(i)}}{2}(z_i^2 - z_{i-1}^2), \quad I_2^{(i)} = \frac{\rho_S^{(i)}}{3}(z_i^3 - z_{i-1}^3)$$

In the same way, using its definition $(\int_{\Omega_S}\boldsymbol{\sigma}^*(\mathbf{u},\omega):\boldsymbol{\varepsilon}(\delta\mathbf{u})\,\mathrm{d}v)$ and combining Eqs. (48) and (52), the elementary elastic stiffness matrix is given by

$$\mathbf{K}_u^{e*} = \sum_{i=1}^{3}\mathbf{K}_{ui}^e + \mathbf{K}_{u\gamma}^e$$

where

$$\mathbf{K}_{ui}^e = \int_{-1}^{1}\int_{-1}^{1}\mathbf{B}_\varepsilon^T\mathbf{C}_i\mathbf{B}_\varepsilon J(\xi,\eta)\,\mathrm{d}\xi\mathrm{d}\eta \quad \text{and}$$

$$\mathbf{K}_{u\gamma}^e = \int_{-1}^{1}\int_{-1}^{1}\mathbf{B}_\gamma^T\mathbf{R}_2\mathbf{B}_\gamma J(\xi,\eta)\,\mathrm{d}\xi\mathrm{d}\eta$$

and where $\mathbf{C}_i$ is the elasticity matrix of the ith layer given by

$$\mathbf{C}_i = \begin{bmatrix} \mathbf{A}_i & -\mathbf{B}_i & t_i\mathbf{A}_i \\ -\mathbf{B}_i & \mathbf{D}_i & -t_i\mathbf{B}_i \\ t_i\mathbf{A}_i & -t_i\mathbf{B}_i & t_i^2\mathbf{A}_i \end{bmatrix} \quad \text{for } i = 1,3 \quad \text{and}$$

$$\mathbf{C}_2 = \begin{bmatrix} \mathbf{A}_2 & -\mathbf{B}_2 & \mathbf{B}_2 \\ -\mathbf{B}_2 & \mathbf{D}_2 & -\mathbf{D}_2 \\ \mathbf{B}_2 & -\mathbf{D}_2 & \mathbf{D}_2 \end{bmatrix} \tag{57}$$

in which the extensional $\mathbf{A}_i$, bending $\mathbf{D}_i$ and extensional-bending $\mathbf{B}_i$ coupling stiffness matrices of the ith layer of the sandwich plate (see for example [30]) are given by

$$\mathbf{A}_i = \begin{bmatrix} A_{11}^{(i)} & A_{12}^{(i)} & A_{16}^{(i)} \\ A_{12}^{(i)} & A_{22}^{(i)} & A_{26}^{(i)} \\ A_{16}^{(i)} & A_{26}^{(i)} & A_{66}^{(i)} \end{bmatrix}; \quad \mathbf{B}_i = \begin{bmatrix} B_{11}^{(i)} & B_{12}^{(i)} & B_{16}^{(i)} \\ B_{12}^{(i)} & B_{22}^{(i)} & B_{26}^{(i)} \\ B_{16}^{(i)} & B_{26}^{(i)} & B_{66}^{(i)} \end{bmatrix}; \quad \mathbf{D}_i = \begin{bmatrix} D_{11}^{(i)} & D_{12}^{(i)} & D_{16}^{(i)} \\ D_{12}^{(i)} & D_{22}^{(i)} & D_{26}^{(i)} \\ D_{16}^{(i)} & D_{26}^{(i)} & D_{66}^{(i)} \end{bmatrix} \tag{58}$$

with

$$A_{mn}^{(i)} = \overline{Q}_{mn}^{(i)}(z_i - z_{i-1}),\quad B_{mn}^{(i)} = \frac{1}{2}\overline{Q}_{mn}^{(i)}(z_i^2 - z_{i-1}^2),\quad D_{mn}^{(i)} = \frac{1}{3}\overline{Q}_{mn}^{(i)}(z_i^3 - z_{i-1}^3)$$

where $m,\ n = 1,2,6$ and $\overline{Q}_{mn}^{(i)}$ represent the reduced material stiffness constants for each layer i in the global coordinate system deduced from the assumption of zero normal stress in the thickness direction.

Finally, the elasticity matrix $\mathbf{R}_2$ related to the shear stresses in the core is given by:

$$\mathbf{R}_2 = h_2 \begin{bmatrix} \overline{Q}_{44}^{(2)} & \overline{Q}_{45}^{(2)} \\ \overline{Q}_{45}^{(2)} & \overline{Q}_{55}^{(2)} \end{bmatrix} \tag{59}$$

6. Numerical examples

In this last section, numerical results, obtained with a Matlab program developed by the authors, are proposed in order to validate and analyze results computed from the proposed formulations. The first two examples concern the free vibration of an undamped then a damped sandwich plate. The structure is discretized using the proposed plate sandwich element. In the damped case, the Modal Strain Energy (MSE) is used in order to compute the eigenfrequencies and the associated modal loss factors. The obtained results are compared to experiments and other numerical solutions which validate and demonstrate the effectiveness of the proposed sandwich plate element. The third example concerns sound transmission through a double-plate system filled with air. In this example, we analyze the air gap effect on the natural vibration of the coupled system and the sound attenuation. The accuracy of model predictions is checked against existing test data. Finally, the transmission loss factor of a double laminated glazing panels with a thin interlayer of PVB is presented. This last example shows the performance of the proposed modal reduction method compared to direct approach and analyzes the effect of the damped PVB viscoelastic layer on noise attenuation.

6.1. Natural frequencies of undamped sandwich plate

In order to validate the proposed finite element sandwich plate formulation, this example gives a comparison of the natural frequencies of a simply supported rectangular sandwich plate with aluminum face layers and a soft orthotropic core. The plate in-plane dimensions are (1.829 m × 1.219 m), the thickness for the face layers is 0.406 mm, and for the core is 6.35 mm. The aluminum face layers are isotropic with elastic properties $E = 70.23$ GPa, $\nu = 0.3$ and material density $\rho = 2820$ kg/m^3. The orthotropic soft core is characterized by the following properties $E_1 = E_2 = 137$ MPa; $G_{12} = 45.7$ MPa; $G_{13} = 137$ MPa; $G_{23} = 52.7$ MPa; $\nu_{12} = 0.5$ and $\rho = 124.1$ kg/m^3.

Table 1
First ten natural frequencies (Hz) for the undamped rectangular sandwich plate.

Mode	Experimental [31]	Rikards et al. [31]	Araújo et al. [4]	Ferreira et al. [14]	Present
1	–	23.4	23.5	23.26	23.25
2	45	45.4	44.8	44.60	44.52
3	69	72.2	71.7	70.27	71.43
4	78	81.6	79.5	79.90	80.02
5	92	95.9	92.5	91.08	91.82
6	129	133.7	126.5	125.51	126.02
7	133	134.2	126.8	128.85	129.80
8	152	152.2	150.7	145.16	151.79
9	169	156.8	170.7	165.16	170.73
10	177	190.9	173.0	173.29	174.17

The first ten natural frequencies are calculated with the present finite element model using 10 × 10 mesh and compared in Table 1 to: (i) experimental results from [31], (ii) 6-nodes FEM results using laminated superelements formed by superposition of plate elements for each layer [31], (iii) serendipity element using a Mindlin theory for the faces and a higher-order approach for the core [4], and (iv) nine nodes layerwise plate finite element developed via an unified formulation [14]. The results obtained with the present element, with only 4 nodes and 7 dofs per node, are in good agreement and convergence with the other solutions.

6.2. Natural frequencies of sandwich plate with a constant complex core's modulus

In this example, a rectangular MPM (metal–polymer–metal) sandwich plate with a constant complex core's modulus is considered. Many investigations have already dealt with the considered plate. The associated geometrical and mechanical data are presented in Table 2.

The Modal Strain Energy is used in this example in order to compute the complex eigenfrequencies and modal loss factors. It assumes that the damped system can be represented in terms of the real normal modes $(\omega_{si}, \mathbf{\Phi}_{si})$ of the associated undamped system given by Eq. (20). Thus, the complex eigenfrequency can be obtained from the following relation

$$(\Omega_{si}^*)^2 = \frac{\mathbf{\Phi}_{si}^T \mathbf{K}_u^* \mathbf{\Phi}_{si}}{\mathbf{\Phi}_{si}^T \mathbf{M}_u \mathbf{\Phi}_{si}} = \Omega_{si}^2(1 + i\eta_{si}) \tag{60}$$

where Ω_{si} is the real part of the complex eigenfrequency and η_{si} is the corresponding modal loss factor.

Table 3 compares the natural frequencies and modal loss factors predicted by the developed element using 10 × 10 mesh to: (i) an analytical solution [17], (ii) a finite element approach based on Von Kármán plate theory in order to describe the nonlinear geometrical effect and on Mindlin's theory to reflect the shear deformation in the viscoelastic layer [7], and (iii) the nine nodes layerwise plate finite element developed by Ferreira et al. in [14]. The results obtained by the present approach are in concordance with those of [7] for simply-supported case (SSSS) and they are very close to the analytical ones presented in [17] for clamped case (CCCC). For this particular example and concerning the computation time, we compared the results of our element to those obtained with Nastran using 10 Quad4 elements for each face and 10 × 5 Hex8 elements for the core (in order to take into account the transverse shear effect). Besides the good convergence in terms of frequencies, this comparison showed that our formulation is much more faster than Nastran (CPU time about 8).

These first two examples validate the development of the proposed finite element sandwich plate with viscoelastic core and show its efficiency compared to other richer elements.

Table 2
Geometrical and mechanical data of sandwich plate with a constant complex core's modulus.

Geometrical data		
Lenght	348 mm	
Width	304.8 mm	
Face's thickness	0.762 mm	
Core's thickness	0.254 mm	
	Elastic faces	Polymer core
Mechanical data		
Young's modulus	6.89×10^{10} Pa	2670.08×10^3 Pa
Poisson ratio	0.3	0.49
Mass density	2740 kg/m^3	999 kg/m^3
Loss factor	–	0.5

Table 3
First five natural frequencies (Hz) and associated loss factors for the sandwich plate with a constant complex core's modulus.

Analytical [17]		Bilasse [7]		Ferreira [14]		Present	
f (Hz)	η	f (Hz)	η	f (Hz)	η	f (Hz)	η
SSSS							
60.3	0.190	58.0	0.170	58.61	0.185	57.82	0.170
115.4	0.203	113.8	0.193	112.253	0.205	113.53	0.191
130.6	0.199	129.5	0.192	127.00	0.202	129.14	0.190
178.7	0.181	177.2	0.172	173.42	0.186	175.84	0.169
195.7	0.174	194.6	0.169	189.83	0.179	195.53	0.165
CCCC							
87.4	0.189	87.4	0.189	85.05	0.192	87.78	0.187
148.9	0.165	148.9	0.164	144.55	0.170	150.43	0.161
169.9	0.154	170.3	0.153	164.69	0.160	171.99	0.150
223.9	0.139	223.9	0.139	216.56	0.146	225.47	0.134
241.0	0.134	241.1	0.134	233.16	0.141	246.96	0.127

6.3. Sound transmission through an elastic double-panel system

In this section, the validation of the proposed coupled finite elements formulation for sound radiation is presented. The problem under consideration is shown in Fig. 4. A normal incidence plane wave excites a double-plate system filled with air (density $\rho_F = 1.21$ kg/m^3 and speed of sound $c_F = 340$ m/s). The plane wave has a pressure amplitude of 1 N/m^2 and is applied to plate 1 as the only external force to the system. The plates are identical and simply supported with thicknesses of 1 mm. The density of the plates is 2814 kg/m^3, the Youngs modulus is 71 GPa, the Loss factor is 0.01 and Poisson ratio 0.33. The surrounding fluid is the air. This example was originally proposed by Panneton in [27].

Concerning the finite element discretization, we have used, for the structural part, 10×10 rectangular elements for each plate. The acoustic cavity is discretized using $10 \times 10 \times 5$ hexahedric elements. The structural and acoustic meshes are compatible at the interface. For more details about the hexahedric acoustic element and the associated fluid–structure coupling element, we refer the reader to [20].

When the excitation is applied to the first plate, the second one vibrates and radiates sound caused by the coupling of air and plate 1. The normal incidence sound transmission loss is then computed using the Rayleigh's integral method which needs the finite element solution of surface velocities of plate 2. For this purpose, the resolution of the coupled system is done with a modal reduction approach using the first 10 in vacuo structural modes and the first 10 acoustic modes of the fluid in rigid cavity.

Fig. 5 shows the normal incidence transmission loss through a simply supported plate (dashed line). Due to the modal behavior of the plate, dips in the transmission loss curve are observed at its resonance frequencies (modes (1,1), (3,1) and (1,3)). When a second plate is used to form an airtight cavity (continuous line), an increase in the transmission loss is achieved except in the region of the so-called plate–cavity–plate resonance (mode $(1,1)^*$). At this frequency, the two plates move out of phase with each other and the effect of the cavity on the plates is mostly one of added stiffness. This frequency is similar to the mass–air–mass resonance of unbounded double panels analyzed in the next section. The frequencies and the mode shapes of these coupled modes are presented in Table 4 and Fig. 10. Table 4 shows also a comparison between the present results and those given by the finite element code Nastran using the same mesh. These results show the excellent performance of the developed finite element model compared to Nastran and enable us to check the validity of the fluid–structure proposed formulation. In addition, the variation of the nSTL of an air-filled panels and a simple panel is in very good agreement with the published date from [27] which validates the development of the proposed acoustic indicators. Note that the influence of several key parameters on the sound isolation capability of the double-panel configuration including panel dimensions, thickness of air cavity, elevation angle, and azimuth angle of incidence sound is not the purpose of this study and can be found in [35].

Fig. 6 presents a comparison of the normal incidence sound transmission through an air-filled finite double panel and an air-filled infinite double panel computed from an analytical solution given in [12,5]. For unbounded panels, the first dip occurs at the mass–air–mass frequency ($f_{mam} = 181.63$ Hz) given by the formula:

$$f_{mam} = \frac{1}{2\pi}\sqrt{\frac{\rho_F c_F^2}{d}\,\frac{m_{S1}+m_{S2}}{m_{S1}m_{S2}}} \tag{61}$$

where d is the panel spacing and m_{S1} and m_{S2} are the surface mass densities of the panels.

At this frequency, the two plates vibrate, as it were, on the stiffness of the air layer. For low frequencies up to the mass–air–mass

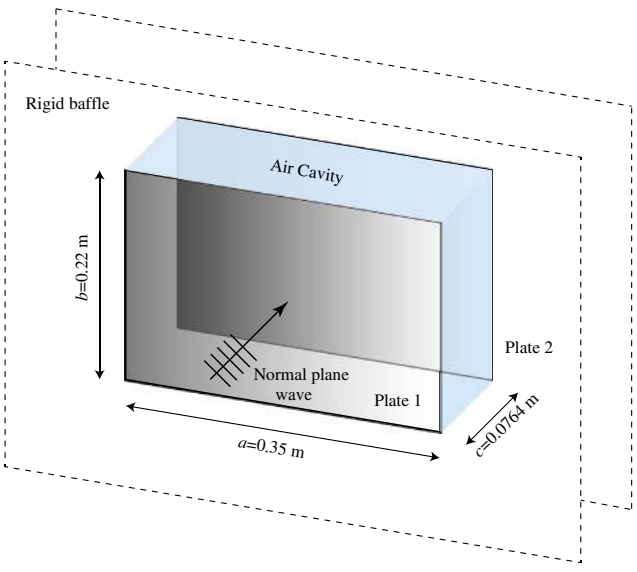

Fig. 4. Double-plate system filled with air: geometric data.

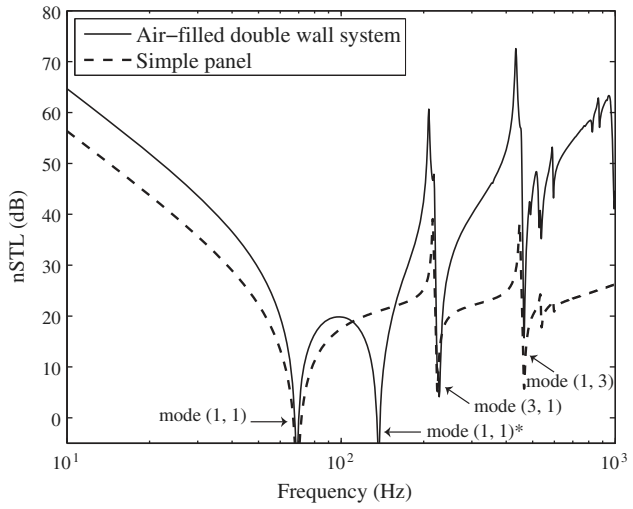

Fig. 5. Comparison of the normal incidence sound transmission (nSTL) through an air-filled double panel and a simple panel.

Table 4
List of the coupled mode eigenfrequencies.

Mode	Nastran	Present	Type of mode
(1,1)	68.69	69.14	Structure
(1,1)*	153.58	148.79	Coupled
(3,1)	220.75	224.39	Structure
(1,3)	462.50	464.72	Structure

frequency, the transmission loss follows the so-called mass law: the two plates are coupled in such a way that the plates vibrate as if they were a single plate with the total mass of the two plates and the transmission loss increasing with frequency at 6 dB per octave and 6 dB when the mass is doubled. It's clear from this comparison that the unbounded model is attractive to use for the prediction of global trends at higher frequencies, but is unsuitable to use for predictions in the small frequency bands and around eigenfrequencies of the double wall panel [5].

6.4. Sound transmission through a double laminated glazing panels

The proposed reduced order finite-elements formulation is applied now to calculate the transmission loss factor of a double laminated glazing panels. The system consists of two identical clamped laminated panels of glass (in-plane dimensions are $L_x = 0.45$ m and $L_y = 1.2$ m) separated by an air cavity of 12 mm thickness. Each laminated glass is composed of two glass plates bonded together by a PVB interlayer. The thickness of outer and inner glass ply is $h_1 = h_3 = 3$ mm and those of the PVB interlayer is $h_2 = 1.14$ mm. The glass ply is modeled as linear elastic material (density 2500 kg/m^3, Youngs modulus 72 GPa, and Poisson ratio 0.22). The material properties of the PVB are both thermal and frequency dependent. From dynamic and thermal tests, Havrillak and Negami have found an empirical law describing this dependence. The resulting complex frequency dependent shear modulus of the PVB is given at 20 °C as [16,18]:

$$G^*(\omega) = G_\infty + (G_0 - G_\infty)\left[1 + (i\omega\tau_0)^{1-\alpha_0}\right]^{-\beta_0} \tag{62}$$

where $G_\infty = 0.235$ GPa, $G_0 = 0.479$ Mpa, $\alpha_0 = 0.46$, $\beta_0 = 0.1946$, $\tau_0 = 0.3979$. The Poisson ratio of the PVB is 0.4 and density is 999 kg/m^3. Concerning the excitation and the finite element discretization, we used the same ones as in the previous example.

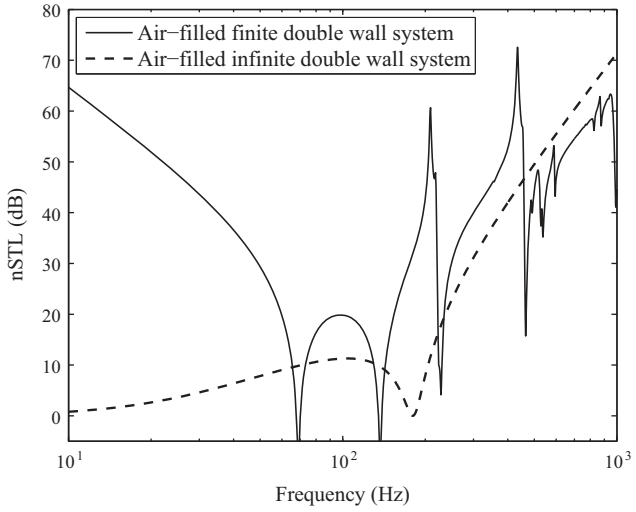

Fig. 6. Comparison of the normal incidence sound transmission (nSTL) through an air-filled finite double panel (finite element result) and an air-filled infinite double panel (analytical solution).

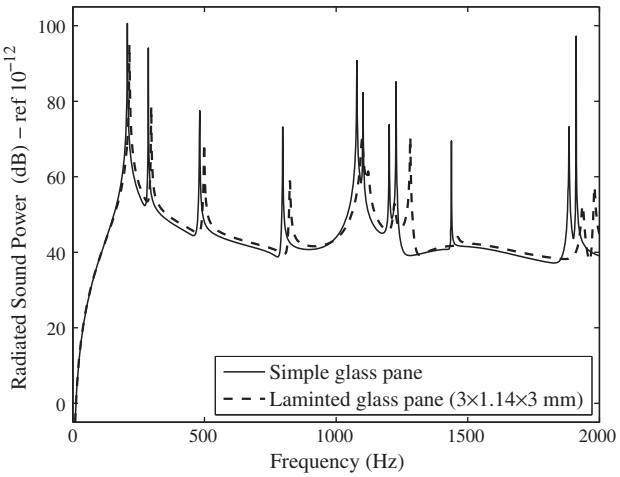

Fig. 7. Comparison of radiated sound power from a simple glass pane and a laminated glass with the same mass.

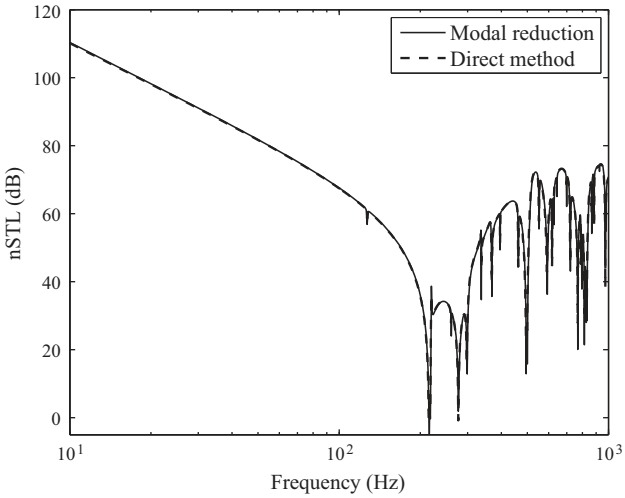

Fig. 8. nSTL through an air-filled double panel: comparison between the modal reduction approach and the direct nodal method.

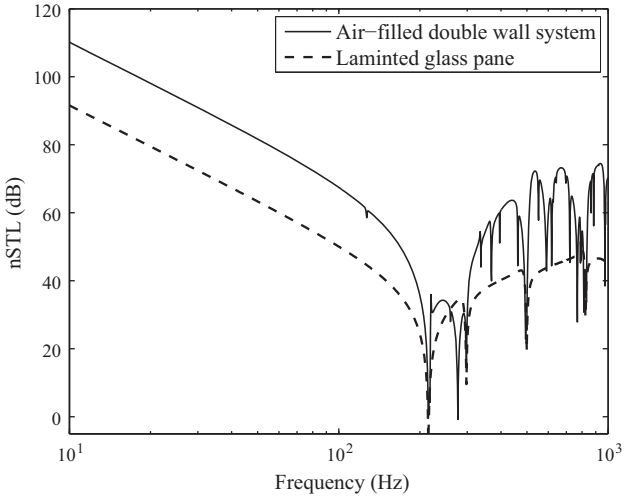

Fig. 9. Comparison of the normal incidence sound transmission (nSTL) through an air-filled double laminated panel and a single laminated panel.

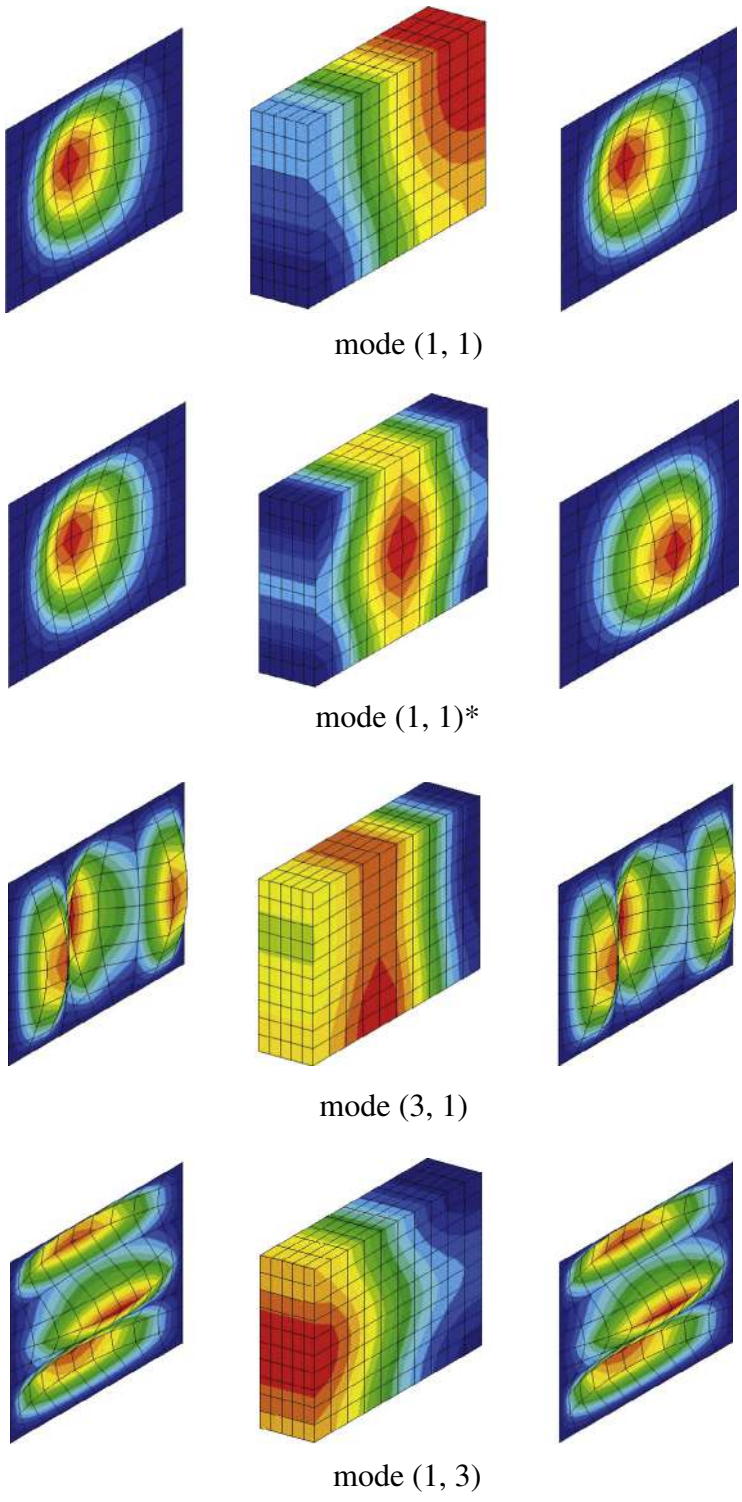

Fig. 10. Fluid–structure coupled modes (fluid pressure and panels total displacement): in phase modes (1,1), (3,1) and (1,3) and out of phase mode (1,1)*.

A comparison between a simple glass and a laminated glass with PVB interlayer with an equivalent surface mass is shown in Fig. 7. Calculation was limited to 2000 Hz maximum. This comparison shows that laminated glass has a much lower acoustic radiation compared to conventional glass at resonance frequencies du to the effect of the viscoelastic layer. The reduction of sound radiation power is around 10 dB in lower frequencies and around 20 dB in higher frequencies. In fact, at low frequencies, the viscoelastic material is soft and the damping is small. At higher frequencies, the stiffness decreases rapidly and the damping is highest. Moreover, flexural vibrations causes shear strain in the viscoelastic core which dissipates energy and reduces vibration and noise radiation. Note that the thickness of the viscoelastic layer has a significant influence in terms of attenuation.

Fig. 8 shows a comparison between the nSTL of the coupled problem, obtained with the proposed modal reduction approach with a truncation on the first twenty structural modes ($N_s = 20$) and first twenty acoustic modes ($N_f = 20$) and the direct nodal

method (Eq. (17)) where the displacement and pressure vectors are calculated for each frequency step. The structural modes are calculated from Eq. (20) using the constant shear storage modulus G_∞ but of course for the computation of the response, the complex stiffness matrix is used with $G^*(\omega)$ (the structural modes, which are real, are only used as a projection bases). As can be seen, a very good agreement between the two methods is proved. Note that, in order to evaluate the number of modes to keep in the modal projection, various simulations have been performed with the proposed static correction and twenty were sufficient by comparison with direct finite element analysis in the frequency range of interest. In this respect, the resulting reduction of the model size and the computational effort using the reduced order method are very significant compared to those of the direct approach. For this particular example, the comparisons of computational times (using an implementation of the two methods in the Matlab software) showed that reduced order model is much more faster than the direct technique (the CPU time ratio is about 15, for an initial problem which has more than 2000 degrees of freedom to a reduced order problem which has 40 degrees of freedom).

In Fig. 9, the nSTL versus frequency curves of the single and double laminated panels are plotted together. A significant reduction of sound is achieved with the presence of the air cavity between the panels compared to the single panel. By introducing a thin PVB interlayer within the panels, we provide better insulation due to a reduction in coincidence dips.

7. Conclusions

In this paper, a finite element formulation for sound transmission through double wall sandwich panels with viscoelastic core is presented. A reduced-order model, based on a normal mode expansion, is then developed. The proposed methodology requires the computation of the eigenmodes of the undamped structure, and the rigid acoustic cavity. A static corrections are introduced in the modal bases in order to take into account the effect of the higher modes. Despite its reduced size, this model is proved to be very efficient for simulations of steady-state analyses of structural–acoustic coupled systems with viscoelastic interlayers when appropriate damping terms are inserted into the modal equations of motion. The Rayleigh integral method is then used in order to estimate the normal sound transmission loss factor of the system. Finally, an efficient finite element sandwich plate which takes into account the influence of the transversal shearing in the core is developed. Various results are presented in order to validate and illustrate the efficiency of the proposed finite element formulations. Further investigations will concern introduction of passive dissipation in the fluid and active one in the structure using piezoelectric materials.

References

[1] Akrout A, Karra C, Hammami L, Haddar M. Viscothermal fluid effects on vibro-acoustic behaviour of double elastic panels. Int J Mech Sci 2008;50(4):764–73.

[2] Akrout A, Hammami L, Ben Tahar M, Haddar M. Vibro-acoustic behaviour of laminated double glazing enclosing a viscothermal fluid cavity. Appl Acoust 2009;70(1):82–96.

[3] Alam N, Asnani NT. Vibration and damping analysis of multilayered rectangular plates with constrained viscoelastic layers. J Sound Vib 1984;97 (4):597–614.

[4] Araújo AL, Mota Soares CM, Mota Soares CA. Finite element model for hybrid active–passive damping analysis of anisotropic laminated sandwich structures. J Sandw Struct Mater 2010;12(4):397–419.

[5] Basten TGH. Noise reduction by viscothermal acousto-elastic interaction in double wall panels, Ph.D.-thesis. University of Twente, Enschede, The Netherlands; 2001.

[6] Beranek LL, Work GA. Sound transmission through multiple structures containing flexible blankets. J Acoust Soc Am 1949;21(4):419–28.

[7] Bilasse M, Azrar L, Daya EM. Complex modes based numerical analysis of viscoelastic sandwich plates vibrations. Comp Struct 2011;89(7–8):539–55.

[8] Bouayeda K, Hamdi MA. Finite element analysis of the dynamic behavior of a laminated windscreen with frequency dependent viscoelastic core. J Acoust Soc Am 2012;132(2):757–66.

[9] Craik RJM. Non-resonant sound transmission through double walls using statistical energy analysis. Appl Acoust 2003;64:325–41.

[10] Deü J-F, Larbi W, Ohayon R. Piezoelectric structural acoustic problems: symmetric variational formulations and finite element results. Comp Meth Appl Mech Eng 2008;197(19–20):1715–24.

[11] Dijckmans A, Vermeir G, Lauriks W. Sound transmission through finite lightweight multilayered structures with thin air layers. J Acoust Soc Am 2010;128(6):3513–24.

[12] Fahy F. Sound and structural vibration. 1st ed. New York: Academic Press; 1985.

[13] Fan Z. Transient vibration and sound radiation of a rectangular plate with viscoelastic boundary supports. Int J Numer Meth Eng 2001;51:619–30.

[14] Ferreira AJM, Araújo AL, Neves AMA, Rodrigues JD, Carrera E, Cinefra M, et al. A finite element model using a unified formulation for the analysis of viscoelastic sandwich laminates. Compos Part B: Eng 2013;45(1):1258–64.

[15] Foss RV, Dear TA, Hamdi MA, Assaf S. Facade noise control with glass and laminates. Glass Process Days 1999;13–16(June):424–31.

[16] Havriliak S, Negami S. A complex plane analysis of dispersions in some polymer systems. J Polym Sci Part C: Polym Symp 1966;14(1):99–117.

[17] Johnson C, Kienholz D. Finite element prediction of damping in structures with constrained viscoelastic layers. Am Inst Aeronaut Astronaut 1982;20:128–490.

[18] Koutsawa Y, Azoti WL, Belouettar S, Martin R, Barkanov E. Loss behavior of viscoelastic sandwich structures: a statistical-continuum multi-scale approach. Compos Struct 2012;94(4):1391–7.

[19] Larbi W, Deü J-F, Ohayon R. Vibration of axisymmetric composite piezoelectric shells coupled with internal fluid. Int J Numer Meth Eng 2007;71 (12):1412–35.

[20] Larbi W, Deü J-F, Ohayon R. Finite element formulation of smart piezoelectric composite plates coupled with acoustic fluid. Compos Struct 2012;94 (2):501–9.

[21] Larbi W, Deü J-F, Ohayon R. Reduced order finite element models for sound transmission analysis through a double sandwich panel with viscoelastic core. In: Topping BHV, Iványi P, editors. Proceedings of the twelfth international conference on computational structures technology. Stirlingshire (UK): Civil-Comp Press; 2014. p. 229. http://dx.doi.org/10.4203/ccp.106.229.

[22] London A. Transmission of reverberant sound through double walls. J Acoust Soc Am 1950;22(2):270–9.

[23] Melosh RJ. Structural analysis of solids. J Struct Div, Proc Am Soc Civil Eng 1963:205–23.

[24] Morand HJ-P, Ohayon R. Fluid–structure interaction. New York: John Wiley & Sons; 1995.

[25] Ohayon R. Reduced models for fluid–structure interaction problems. Int J Numer Meth Eng 2004;60(1):139–52.

[26] Ohayon R, Soize C. Advanced computational vibroacoustics: reduced-order models and uncertainty quantification. Cambridge University Press; 2014.

[27] Panneton R. Modélisation numérique tridimensionnelle par éléments finis des milieux poroélastiques: application au problème couplé lasto-poro-acoustique, Ph.D. Université de Sherbrooke; 1996.

[28] Quirt JD. Sound transmission through windows I. Single and double glazing. J Acoust Soc Am 1982;72(3):834–44.

[29] Quirt JD. Sound transmission through windows II. Double and triple glazing. J Acoust Soc Am 1983;74(2):534–42.

[30] Reddy JN. Mechanics of laminated composite plates and shells: theory and analysis. 2nd ed. Boca Raton (FL): CRC Press; 2004.

[31] Rikards R, Chate A, Barkanov E. Finite element analysis of damping the vibrations of laminated composites. Comp Struct 1993;47(6):1005–15.

[32] Sgard FC, Atalla N, Nicolas J. A numerical model for the low frequency diffuse field sound transmission loss of double-wall sound barriers with elastic porous linings. J Acoust Soc Am 2000;108(6):2865–72.

[33] Tadeu AJB, Mateus Diogo MR. Sound transmission through single, double and triple glazing. Experimental evaluation. Appl Acoust 2001;62:307–25.

[34] Vasques CMA, Moreira RAS, Dias Rodrigues J. Viscoelastic damping technologies. Part I: modeling and finite element implementation. J Adv Res Mech Eng 2010;1(2):76–95.

[35] Xin FX, Lu TJ, Chen CQ. Vibroacoustic behavior of clamp mounted double-panel partition with enclosure air cavity. J Acoust Soc Am 2008;124(6):3604–12.

[36] Zienkiewicz OC, Taylor RL. The finite element method. The basis, vol. 1. Butterworth-Heinemann; 2001.